Corrosion Resistance of Zinc Phosphated HRB400 Steel in Simulated Concrete Pore Solution

Guan Xiaoyan[1],*, Jiao Huili[2]

[1] Department of Architectural Engineering, Shijiazhuang University of Applied Technology, Shijiazhuang 050081, China;
[2] Project Management, CSCEC Road and Bridge Group Technology Development Co., Ltd, Shijiazhuang 050020, China
*E-mail: sjzpt_edu@126.com

HRB400 steel samples were treated by zinc, zinc-manganese and zinc-calcium phosphating technique. The corrosion resistance of zinc phosphated HRB400 steel in simulated concrete pore solution was investigated based on polarization curve and electrochemical impedance spectra. The results show that phosphating treatment could mitigate HRB400 steel corrosion. Specifically, black-gray and tightly bound zinc, zinc-manganese or zinc-calcium phosphating coating formed on the surface of HRB400 steel, blocking its contact with the corrosion media and inhibiting the corrosion reaction. The phosphating coatings exhibited different morphology and compactness, as well as different corrosion resistance. Compared with zinc and zinc-calcium phosphating coating, zinc-manganese phosphating coating exhibited the optimal compactness and minimum corrosion current density of 1.15×10^{-6} A/cm^2, the maximum charge transfer resistance of 7712.6 $\Omega \cdot$cm^2 and low-frequency impedance value of 6006.4 $\Omega \cdot$cm^2, providing excellent corrosion protection of HRB400 steel. Overall, the zinc-manganese phosphated HRB400 steel showed the best corrosion resistance in simulated concrete pore solution, making its wide application in reinforced concrete structures.

1. INTRODUCTION

Reinforced concrete structures are composed of rebars and concrete, which can withstand high tension and pressure through strong bonding. Reinforced concrete structures have been widely used because of their high stability, good fireproof performance and low cost. However, the rebar and concrete durabilities are limited because rebars in the reinforced concrete are the main sources of premature failure for reinforced concrete structures [1-6]. Due to concrete carbonization and diffusion

of chloride ions in the surrounding environment, rebars are readily exposed to the local erosion and electrochemical corrosion. Therefore, it is important to take measures to improve the corrosion resistance of rebars in reinforced concrete to ensure the durability of reinforced concrete structures.

Among various feasible measures to mitigate this problem, phosphating seems to be the most easy-to-operate and cost-effective solution. As an environmental friendly coating, phosphating coating can act as a physical barrier to isolate corrosion media and inhibit the formation of micro-scale batteries on the metal surface, effectively preventing electrochemical corrosion [7-12]. However, the mechanism of phosphated rebar corrosion resistance needs a deeper insight. In this study, HRB400 steel was treated by different phosphating techniques. The corrosion resistance of zinc phosphated HRB400 steel in the saturated calcium hydroxide solution with added sodium chloride and sodium silicate, which simulated the concrete pore environment, was investigated to provide a reference for improving the durability of reinforced concrete structures.

2. MATERIALS AND METHODS

2.1 Materials

This study used HRB400 steel with the following composition: C=0.17~0.24%, Si=0.17~0.37%, Mn=1.3~1.6%, Ti=0.04~0.1%, P=0.035%, Ce=0.03%, and the rest being Fe. HRB400 steel blank was cut into multiple samples with a diameter of 14 mm and a length of 60 mm to facilitate the experiment. First, coarse and fine sandpaper grades were used to polish the samples step-by-step to remove the oxide scale and rust layer from their surface. Next, a hot alkaline solution (sodium hydroxide 45 g/L, 60°C) was used to remove the oil, and the sample was then soaked in a 10% hydrochloric acid for activation. Finally, the sample was washed with deionized water, dried, and placed into the constant-temperature drying box.

2.2 HRB400 steel phosphating treatment

HRB400 steel samples were treated by zinc, zinc-manganese and zinc-calcium phosphating technique. These samples were denoted as zinc, zinc-manganese and zinc-calcium phosphated HRB400 steel, respectively. The as-prepared phosphating coatings were denoted as zinc, zinc-manganese and zinc-calcium phosphating coating, respectively. Table 1 lists the solution composition and technique conditions used in the above phosphating technique. Herein, the same thickness of different phosphating coatings was obtained by adjusting the duration of phosphating.

Table 1. Solution composition and conditions used in different phosphating techniques

Different phosphating technique	Solution composition	Conditions
zinc phosphating	zinc phosphate monobasic 60 g/L, zinc nitrate 45 g/L, sodium fluoride 5 g/L	65°C, 18 min

zinc-manganese phosphating	manganese dihydrogen phosphate 24 g/L, zinc phosphate monobasic 40 g/L, manganese nitrate 60 g/L, zinc nitrate 50 g/L, sodium citrate 1.2 g/L, nickel nitrate 1 g/L, tartaric acid 1 g/L	70°C, 15 min
zinc-calcium phosphating	zinc oxide 8 g/L, phosphoric acid(85%) 16 mL/L, nitric acid(68%) 20 mL/L, calcium carbonate 30 g/L, citric acid 1 g/L, nickel nitrate 0.6 g/L	65°C, 25 min

2.3 Corrosion resistance test

2.3.1 Polarization curve and electrochemical impedance spectra

Saturated calcium hydroxide solution was prepared. Sodium hydroxide solution was first added to adjust the pH to 12.0~12.4, then 0.01 mol/L sodium chloride and 0.005 mol/L sodium silicate were added and stirred well. The above solution was used as to simulate the concrete pore solution. A platinum sheet acted as an auxiliary electrode, while the saturated calomel electrode acted as a reference electrode. HRB400 steel and zinc phosphated HRB400 steel samples were used as working electrodes. The preparation method of the working electrode was as follows: the sample was cut and then shaped, edge polished and treated with sealing wax to prepare the working electrode with an exposed area of 1 cm^2. After each electrode reached the steady state after being immersed in the simulated concrete pore solution, the polarization curve was constructed at a scan rate of 1 mV/s. The electrochemical impedance spectra are tested with the AC disturbance signal amplitude of 10 mV, and frequency range from 100 kHz to 10 mHz. An electrochemical workstation (CHI760E) was used to analyze the polarization curve and electrochemical impedance spectra.

2.3.2 Effect of immersion time on corrosion resistance

The HRB400 steel and zinc phosphated HRB400 steel samples were immersed in simulated concrete pore solution for 2, 5, 9, 14, 17 and 21 days, respectively. Multiple samples used in the experiment were dried after each immersion period, and their corrosion weight gain was obtained by weighing with an electronic balance (AX523ZH/E). Additionally, a scanning electron microscopy (MERLIN Compact) was used to observe the surface morphology of the HRB400 steel and zinc phosphated HRB400 steel samples before and after corrosion. An energy dispersive spectroscopy (EDS) was used to analyze the composition of different phosphating coatings.

3. RESULTS AND DISCUSSION

3.1 Surface morphology of zinc phosphated HRB400 steel and composition of different phosphating coatings

The appearance of HRB400 steel and zinc phosphated HRB400 steel are shown in Figure 1. Unlike HRB400 steel, the zinc, zinc-manganese and zinc-calcium phosphated HRB400 steel were black-gray, while all phosphating coatings completely covered HRB400 steel with good adhesion.

(a) HRB400 steel   (b) zinc phosphated HRB400 steel

(c) zinc-manganese phosphated HRB400 steel   (d) zinc-calcium phosphated HRB400 steel
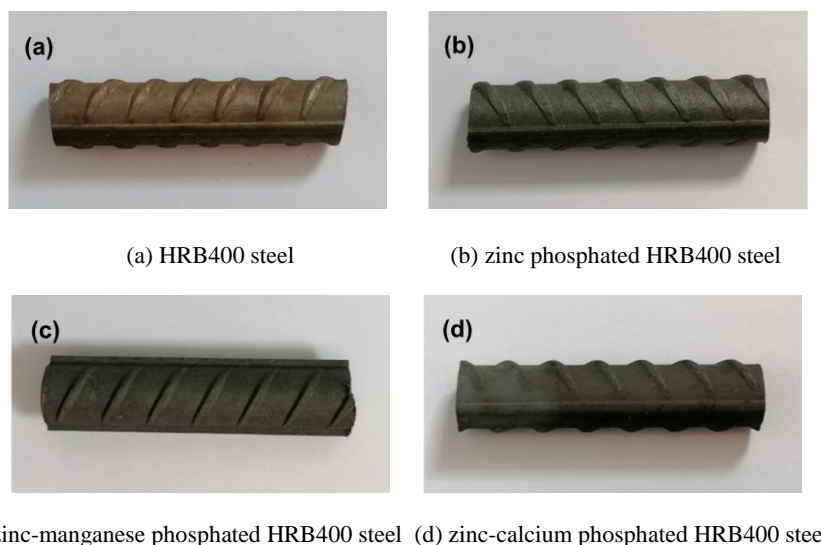
**Figure 1.** Appearance of HRB400 steel and zinc phosphated HRB400 steel

Figure 2(a) shows different depths of wear scars and irregular pits on the HRB400 steel surface formed by grinding and corrosion activation during the pretreatment. According to Figure 2(b), the grain morphology of zinc phosphating coating was irregular. Strip and block grains were stacked alternately with holes and gaps between the grains, and the surface was relatively rough. These holes and gaps will gradually become corrosion channels, harming the corrosion resistance of zinc phosphating coating [13-16]. As shown in Figure 2(c) and 2(d), the morphological characteristics of zinc-manganese and zinc-calcium phosphating coatings differed from those of zinc phosphating coating, and their grain morphology was more regular. Moreover, the formed had long granular grains, and the latter had cellular crystals. Although there were also holes and gaps between the grains of zinc-manganese and zinc-calcium phosphating coatings, their compactness are significantly better than that of zinc phosphating coating. Specifically, zinc-manganese phosphating coating had the optimal compactness.

(a) HRB400 steel   (b) zinc phosphating coating

(c) zinc-manganese phosphating coating   (d) zinc-calcium phosphating coating
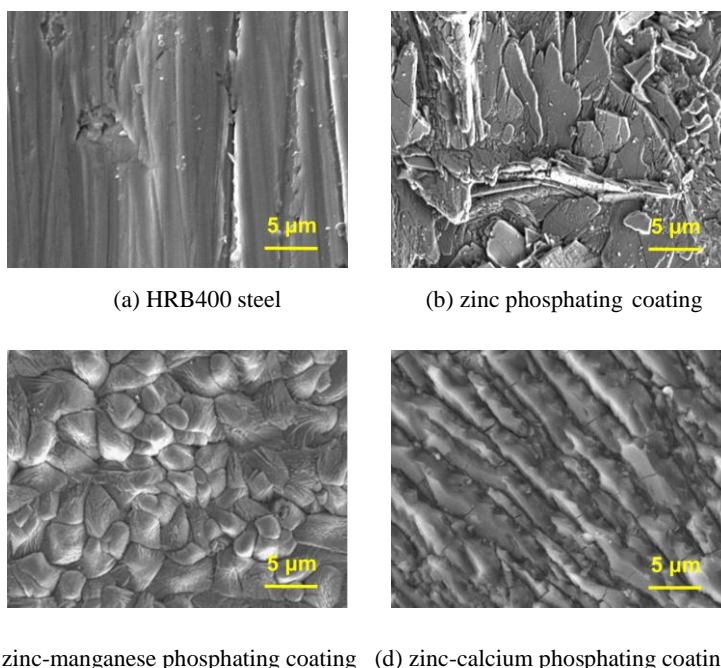
Figure 2. Surface morphology of HRB400 steel and different phosphating coatings

Figure 3 illustrates the composition of different phosphating coatings. As observed, the main composition of zinc phosphating coating were Zn, O, and P, while the mass fraction of Zn and O were both approximately 39%. The main composition of zinc-manganese phosphating coating were Zn, O, Mn, and P, in which the mass fraction of Zn was the highest and that of Mn was the lowest. The main composition of zinc-calcium phosphating coating were Zn, O, Ca, P, Fe and Zn. The mass fraction of Fe was also the highest, and that of Fe was the lowest.


(a) zinc phosphating coating   (b) zinc-manganese phosphating coating
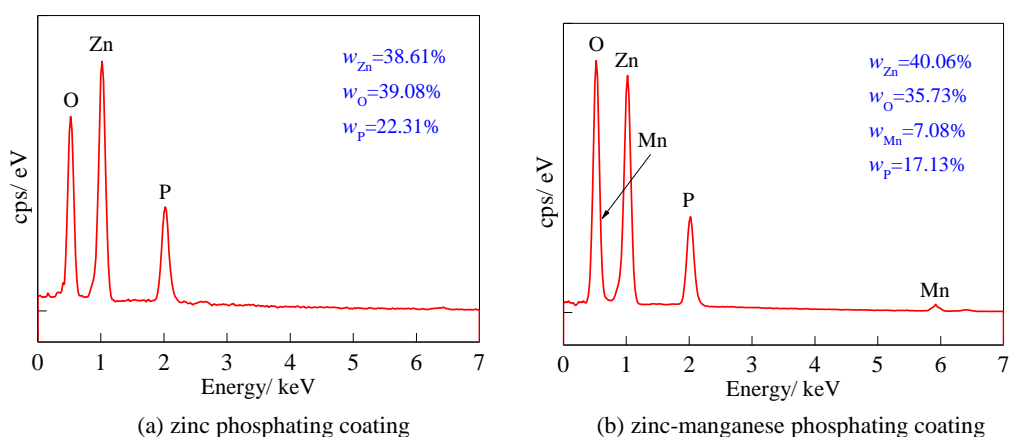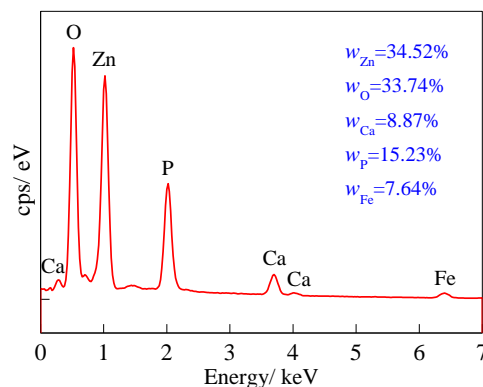
(c) zinc-calcium phosphating coating

Figure 3. Composition of different phosphating coatings

3.2 Polarization curve and electrochemical impedance spectra of HRB400 steel and different phosphating coatings

Figure 4 shows the polarization curve of HRB400 steel and different phosphating coatings in simulated concrete pore solution. Table 2 lists the corrosion potential, corrosion current density and polarization resistance obtained by fitting. In general, the corrosion tendency was judged according to the corrosion potential, it weakened with the increased corrosion potential. The corrosion rate was judged according to the corrosion current density. The smaller corrosion current density, the slower the corrosion [17-20]. According to Figure 4 and Table 2, the corrosion potential of zinc, zinc-manganese and zinc-calcium phosphating coatings shifted by about 60 mV, 120 mV, and 80 mV, respectively, compared to HRB400 steel, suggesting that phosphating treatment weakened the corrosion tendency of HRB400 steel. According to the observed changes in the corrosion current density, it can be concluded that the corrosion rate of zinc, zinc-manganese and zinc-calcium phosphating coatings decreased compared to HRB400 steel, proving that phosphating treatment significantly improved the corrosion resistance of HRB400 steel in simulated concrete pore solution.

Notably, the corrosion potential and corrosion current density of various phosphating coatings differed, indicating that their corrosion resistance significantly varied. The corrosion current density of zinc, zinc-manganese and zinc-calcium phosphating coatings were 4.5×10^{-6} A/cm^2, 1.2×10^{-6} A/cm^2 and 2.8×10^{-6} A/cm^2, while that of HRB400 steel was 3.6×10^{-5} A/cm^2. Hence, it can be concluded that the corrosion resistance of zinc-manganese phosphating coating was better than those of zinc and zinc-calcium phosphating coatings. Zinc-manganese phosphating coating had optimized compactness, enhancing the blocking effect on corrosion media and effectively delaying the corrosion reaction in the phosphating coating/HRB400 steel interface. Hence, the zinc-manganese phosphating coating effectively improved the corrosion resistance of HRB400 steel in simulated concrete pore solution than the other two phosphating coatings of the same thickness.
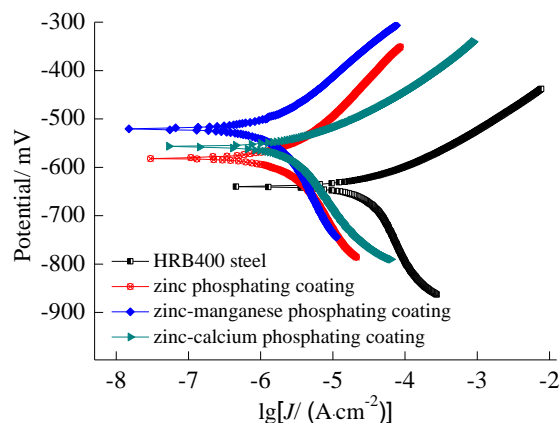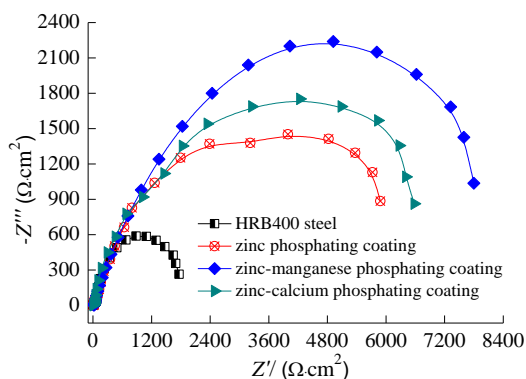
Figure 4. Polarization curve of HRB400 steel and different phosphating coatings in simulated concrete pore solution

Table 2. Corrosion potential and corrosion current density of HRB400 steel and different phosphating coatings

Different samples	Corrosion potential/ mV	Corrosion current density/ (A·cm^{-2})
HRB400 steel	-640	3.6×10^{-5}
zinc phosphating coating	-581	4.5×10^{-6}
zinc-manganese phosphating coating	-520	1.2×10^{-6}
zinc-calcium phosphating coating	-558	2.8×10^{-6}

    To further study the corrosion resistance of zinc phosphated HRB400 steel, the test results on electrochemical impedance spectra were analyzed. Figure 5 shows the electrochemical impedance spectra of the HRB400 steel and different phosphating coatings in simulated concrete pore solution. According to the characteristics of the impedance spectra, an appropriate equivalent circuit was selected for fitting, as shown in Figure 6. Here R_s, R_f, and R_{ct} denote the solution resistance, coating resistance and charge transfer resistance, respectively, Q is the constant phase angle element, while Q_f and Q_{dl} represent the coating and double-layer electric capacitances at the interface between the electrode and solution, respectively. Additionally, the HRB400 steel and different phosphating coatings showed the characteristics of a single capacitive reactance arc. The capacitive reactance arc's radius reflected the corrosion reaction's resistance on the electrode surface: the larger radius, the higher the corrosion resistance [21-25]. Compared with HRB400 steel, the capacitive reactance arc radius of zinc, zinc-calcium and zinc-manganese phosphating coatings increased sequentially, demonstrating their respective ability to hinder charge transfer and electrolyte diffusion.
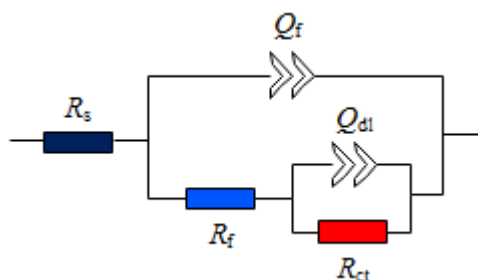
(a) Nyquist graph
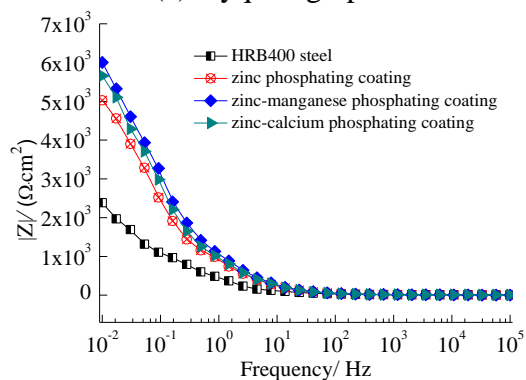
(b) Frequency impedance graph

Figure 5. Electrochemical impedance spectra of HRB400 steel and different phosphating coatings in simulated concrete pore solution


Figure 6. Electrochemical impedance spectra fitting equivalent circuit

According to the electrochemical impedance spectra fitting, the charge transfer resistance of HRB400 steel was 1712.6 $\Omega \cdot cm^2$, and the charge transfer resistance of zinc, zinc-manganese and zinc-calcium phosphating coatings exceeded that of HRB400 steel by 4108 $\Omega \cdot cm^2$, 6000 $\Omega \cdot cm^2$ and 4795 $\Omega \cdot cm^2$, respectively. Meanwhile, and the low-frequency impedance values of zinc, zinc-manganese and zinc-calcium phosphating coatings exceeded that of HRB400 steel (2383.4 $\Omega \cdot cm^2$) by 2644 $\Omega \cdot cm^2$, 3623 $\Omega \cdot cm^2$ and 3275 $\Omega \cdot cm^2$, respectively. In summary, zinc-manganese phosphating coating had the highest values of the capacitive reactance arc radius, charge transfer resistance and low-frequency impedance, indicating its optimal corrosion resistance and the improved corrosion protection of HRB400 steel.

3.3 Corrosion weight gain and corrosion morphology of zinc phosphated HRB400 steel
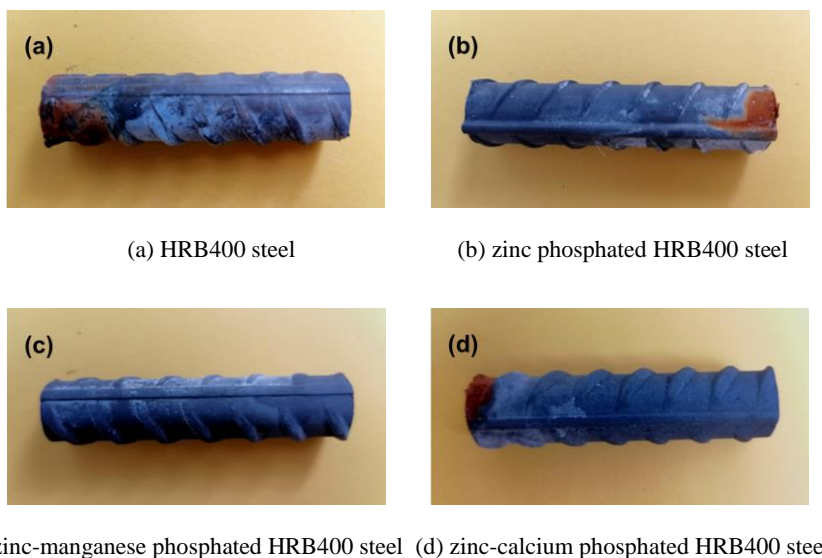
Figure 7 shows the corrosion weight gain of HRB400 steel and zinc phosphated HRB400 steel immersed in simulated concrete pore solution for different periods. As observed, the corrosion weight gain of HRB400 steel immersed in simulated concrete pore solution for 0~9 days increased nearly linearly, indicating that HRB400 steel at this stage corroded faster, and its corrosion degree gradually increased. However, after 9 days, the corrosion weight gain of HRB400 steel decreased and gradually stabilized. This was because the accumulated corrosion products blocked the corrosion process, which was equivalent to inhibiting corrosion [26-28]. The quality of zinc, zinc-manganese and zinc-calcium phosphated HRB400 steel immersed in simulated concrete pore solution for 0~2 days remained unchanged, indicating that the respective coatings well blocked the HRB400 steel erosion at this stage by preventing its direct contact with the concrete solution and hindering its corrosion. However, the corrosion weight gain began to increase after immersion for 2 days, indicating that the zinc, zinc-manganese and zinc-calcium phosphating coatings became corroded. The corrosion degree gradually increased at this stage, varying in zinc, zinc-manganese and zinc-calcium phosphating coatings. Among all phosphated HRB400 steel immersed in simulated concrete pore solution for the same periods, the corrosion weight gain of zinc-manganese phosphated HRB400 steel was lower than that of zinc and zinc-calcium phosphated HRB400 steel.
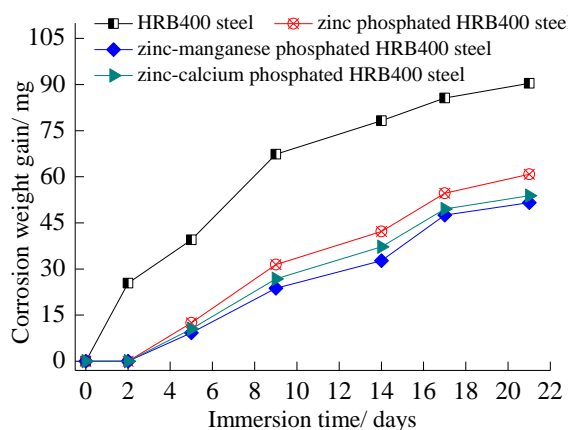
Figure 7. Corrosion weight gain of HRB400 steel and zinc phosphated HRB400 steel immersed in simulated concrete pore solution for different periods

Figure 8 shows the surface morphology of HRB400 steel and zinc phosphated HRB400 steel after immersion in simulated concrete pore solution for 21 days. As observed, HRB400 steel was severely ablated, and a large area of yellow-brown rust was formed on its surface. However, the ablation degree of zinc, zinc-manganese and zinc-calcium phosphated HRB400 steel was significantly reduced, with the yellow-brown rust covering only some local areas. This strongly indicated that phosphating treatment could mitigate the corrosion degree of HRB400 steel and improve its corrosion resistance in simulated concrete pore solution. According to the corrosion weight gain and corrosion morphology, zinc-manganese phosphated HRB400 steel exhibited excellent corrosion resistance in

simulated concrete pore solution. The main reasons were that the compactness of zinc-manganese phosphating coating was improved, and the blocking effect on the corrosion media was improved, promoting the corrosion protection effect on HRB400 steel.

(a) HRB400 steel   (b) zinc phosphated HRB400 steel

(c) zinc-manganese phosphated HRB400 steel (d) zinc-calcium phosphated HRB400 steel

Figure 8. Surface morphology of HRB400 steel and zinc phosphated HRB400 steel after immersion in simulated concrete pore solution for 21 days

4. CONCLUSIONS

This study proved that phosphating treatment can slow down the corrosion reaction of HRB400 steel immersed in simulated concrete pore solution. Black-gray zinc, zinc-manganese or zinc-calcium phosphating coating formed on the HRB400 steel surface provided a tight adhesion, blocking HRB400 steel contact with the corrosion media, inhibiting the corrosion reaction, and improving the corrosion resistance of HRB400 steel in simulated concrete pore solution. The surface morphology and compactness of zinc, zinc-manganese or zinc-calcium phosphating coating differed, providing various corrosion protection effects on HRB400 steel. Compared with zinc and zinc-calcium phosphating coating, zinc-manganese phosphating coating had the optimal compactness, promoting the HRB400 steel corrosion protection. Additionally, zinc-manganese phosphated HRB400 steel exhibited excellent corrosion resistance in simulated concrete pore solution and high application prospects in improving the durability of reinforced concrete structures.

References

1. C. J. Wei, C. S. Wojnar and C. L. Wu, *Cem. Concr. Res.*, 144 (2021) 106404.
2. M. Manera, O. Vennesland and L. Bertolini, *Corros. Sci.*, 50 (2008) 554.
3. K. Kobayashi, K. Hosokawa, Y. Hattori and H. D. Yun, *Cem. Concr. Compos.*, 122 (2021) 104146.
4. E. E. Alami, F. E. Fekak, L. Garibaldi and A. Elkhalfi, *J. Build. Eng.*, 43 (2021) 102789.

5. S. Poyet, W. Dridi, V. L. Hostis and D. Meinel, *Corros. Sci.*, 125 (2017) 48.
6. V. Ramani and K. S. C. Kuang, *Constr. Build. Mater.*, 276 (2021) 122129.
7. J. Chen, H. Y. Yang, G. Q. Xu, P. J. Zhang, J. Lv, W. Sun, B. S. Li, J. Huang, D. M. Wang and Y. C. Wu, *Surf. Coat. Technol.*, 399 (2020) 126115.
8. S. R. Arunima, M. J. Deepa, L. J. Elias, T. R. A. Thara, C. V. Geethanjali and S. M. A. Shibli, *Appl. Surf. Sci.*, 543 (2021) 148822.
9. X. K. Zhao, R. Q. Liu, W. H. Qi and Y. Q. Yang, *Materials*, 16 (2020) 3636.
10. Y. Q. Tian, H. W. Huang, H. H. Wang, Y. H. Xie, X. X. Sheng, L. Zhong and X. Y. Zhang, *J. Alloys Compd.*, 831 (2020) 154906.
11. J. Liu, B. Zhang, W. H. Qi, Y. G. Deng and R. D. K. Misra, *J. Mater. Res. Technol.*, 9 (2020) 5912.
12. X. X. Sun, M. Y. Liu, J. C. Song and Y. S. H. Xu, *Geothermics*, 86 (2020) 101807.
13. A. Palani, B. T. Lu, L. P. Tian, J. L. Luo and Y. C. Lu, *J. Nucl. Mater.*, 396 (2010) 189.
14. A. Nonaka, H. Yamanaka and H. Nonaka, *Int. J. Soc. Mater. Eng. Resour.*, 11 (2008) 1108.
15. H. Tamura, *Corros. Sci.*, 50 (2008) 1872.
16. H. Baba and Y. Katada, *Corros. Sci.*, 48 (2006) 2510.
17. C. Q. Pan, Q. D. Zhong, J. Yang and Y. L. Li, *Surf. Rev. Lett.*, 28 (2021) 2150048.
18. A. Kumar, S. K. Nayak, K. Sarkar, A. Banerjee, K. Mondal and T. laha, *Surf. Coat. Technol.*, 397 (2020) 126058.
19. P. Yu, Z. X. Lian, J. K. Xu and H. D. Yu, *R. Soc. Chem.*, 11 (2021) 847.
20. W. W. Zhang, T. Y. Mei, B. S. Li, L. Yang, S. S. Du, Y. C. Miao and H. Q. Chu, *J. Mater. Res. Technol.*, 12 (2021) 1473.
21. D. G. Tamay, S. Gokyer, J. Schmidt, A. Vladescu, P. Y. Huri, V. Hasirci and N. Hasirci, *ACS Appl. Mater. Interfaces*, 1 (2022) 104.
22. X. Z. Ding, A. L. K. Tan, X. T. Zeng, C. Wang, T. Yue and C. Q. Sun, *Thin Solid coatings*, 516 (2008) 5716.
23. W. C. Kong, Z. Yu and J. Hu, *Diamond Relat. Mater.*, 116 (2021) 108398.
24. J. L. Xu, Q. F. Xiao, D. D. Mei, Y. X. Tong, Y. F. Zheng, L. Li and Z. C. Zhong, *Surf. Coat. Technol.*, 309 (2017) 621.
25. H. Zhang, Y. Zou, Z. D. Zou and C. W. Shi, *J. Rare Earths*, 32 (2014) 1095.
26. Q. Y. Zhao, J. B. Zhao, X. Q. Cheng, Y. H. Huang, L. Lu and X. G. Li, *Surf. Coat. Technol.*, 382 (2020) 125171.
27. R. Solmaz, E. A. Sahin, A. Doner and G. Kardas, *Corros. Sci.*, 53 (2011) 3231.
28. N. Perini, P. G. Corradini, V. P. Nascimento, E. C. Passamani and M. B. J. G. Freitas, *Corros. Sci.*, 74 (2013) 214.